Analysis of Permanent Magnet-assisted Synchronous Reluctance Motor Based on Equivalent Reluctance Network Model

Changbin Li, Xiuhe Wang, *Member, IEEE*, Feng Liu, Jie Ren, Zezhi Xing, and Xinwei Gu

***Abstract*—In this paper, the equivalent reluctance network model (ERNM) is used to calculate the magnetic circuit of a permanent magnet-assisted synchronous reluctance motor (PMASynRM) and calculate no-load air-gap magnetic field and electromagnetic torque. Iteration method is used to solve the relative permeability of iron core. A novel reluctance network model based on actual distribution of the magnetic flux inside the motor is established. The magnetomotive force (MMF) generated by armature winding affects the relative permeability of iron core, which is considered in the calculation of ERNM to improve the accuracy when the motor is under load. ERNM can be used to measure air-gap flux density, no-load back electromotive force (EMF), the average value of motor torque, the armature winding voltage under load, and power factor. The method of calculating the motor performance is proposed. The results of calculation are consistent with finite element method (FEM) and the computational complexity is much less than that of the FEM. The results of ERNM has been verified, which will provide a simple method for motor design and analysis.**

***Index Terms*— Permanent magnet-assisted synchronous reluctance motor (PMASynRM), Equivalent reluctance network model (ERNM), Air-gap flux density, No-load back electromotive force (EMF), Torque.**

I. INTRODUCTION

PERMANENT magnet-assisted synchronous reluctance motor (PMASynRM) combines the characteristics of a permanent magnet synchronous motor and a synchronous reluctance motor. The motors make full use of reluctance torque and permanent magnet torque. The PMASynRM can use a small amount of rare earth material or a low-cost ferrite or bonded NdFeB to achieve the expected performance. PMASynRM have the characteristics with high-power density, high efficiency, wide speed range, small size, and light weight, which are widely used in the industrial drive [1],[2].

The methods often used in motor design include the finite element method (FEM), analytical method and magnetic equivalent circuit (MEC). Using suitable methods in the initial and final stages of motor design can save time and improve the accuracy of the results. When the FEM is used to analyze PMASynRM, complicated magnetic circuit structure and various boundary conditions of the motor can be considered, and the results are accurate. However, FEM is not suitable for making a choice among a wide range of analysis methods due to its consumption of much time and internal memory [3]. Therefore, FEM is usually used in the final verification stage of design models or analytical models [4]-[6]. The analytical method is based on the mathematical description of the geometrical shape of each part of the motor. In [7], the radial and tangential components of air-gap flux density can be accurately obtained by a subdomain field model. When the boundary shape and structure of the electromagnetic field of the motor are more complex, the establishment and solution of the mathematical model in this method will be difficult to establish. MEC has a good coordination between the calculation accuracy and the calculation time, and gradually has been widely used.

In article [8], the air-gap flux density can be obtained from the air-gap flux density of permanent magnets and the air-gap flux density of armature winding, respectively. MEC can be divided into no-load, *d*-axis, and *q*-axis circuits [9]. On the MEC model, the methods for calculating various leakage magnetic permeances are determined according to the motor structure and the leakage reluctances of the magnetic circuit are obtained [10]. An analytical procedure that allows to evaluate the total magnetomotive force (MMF) along *d*-axis, and *q*-axis to improve accuracy in MEC has been proposed in [11]. In article [12], the nonlinear MEC method, which considers the severe magnetic saturation of iron core, is proposed. A MEC model for Synchronous motor incorporating moving air gap and cross-coupled saturation effects proposed in [13]. In article [3], the iterative magnetic circuit calculation is used to deal with the saturation effect of iron core. The lumped magnetic circuit model was extensively used for permanent magnet machine, which derived analytically the air-gap field distribution, average air-gap flux density, and leakage fluxes [4],[14]-[19].

The air gap of motor is an important area for electromechanical energy conversion of motor. The performance and parameters of motor are mostly based on the calculation of air-gap magnetic field. However, the air-gap magnetic field of motor cannot be accurately calculated and the

Manuscript received November 18, 2021; revised January 04, 2022; accepted February 11, 2022. date of publication June 25, 2022; date of current version June 18, 2022.

This work was supported in part by the National Natural Science Foundation of China under Grant 51737008. (*Corresponding author: Xiuhe Wang.*)

Changbin Li, Xiuhe Wang, Feng Liu, Jie Ren, Zezhi Xing, and Xinwei Gu are with the School of Electrical Engineering, Shandong University, Jinan 250061, China (e-mail: ChangbinL@163.com; wangxh@sdu.edu.cn; liucf1019@163.com; renjienh@mail.sdu.edu.cn; xzz_sd001@163.com; guxinwei@mail.sdu.edu.cn).

Digital Object Identifier 10.30941/CESTEMS.2022.00019

important radial component of air-gap flux density cannot be obtained from the traditional MEC [4], [13], [20].

A method called the equivalent reluctance network model (ERNM) is used for the analysis of PMASynRM. Compared with the traditional MEC, the ERNM complies with the principle of minimum reluctance to convert the vector of magnetic flux into a scalar for solution, which improves the accuracy of calculation and is accessible. At the same time, the influences of the placement angle of permanent magnet and iron core in rotor on the air-gap flux density had been solved. The results obtained from the analytical calculation conform well with FEM, and the computation time of the analytical calculation is much less than that of the FEM. The comparison with the no-load air-gap flux density, no-load back electromotive force (EMF), and the average value of motor torque obtained by FEM proves the feasibility and effectiveness of ERNM.

II. Calculation Procedure of the ERNM

In calculation of the ERNM for magnetic circuit, it is assumed that the stator yoke is in an equipotential region of the MMF. The magnetic flux is along the direction of the iron core in the middle of the magnetic barrier and the air-gap MMF changes in radial direction, the flux lines in radial magnetic field region pass vertically through air gap.

A four-pole PMASynRM is used as a prototype, as shown in Fig. 1. Due to the symmetry of the motor structure, ERNM is applied to calculate a quarter of the rotor model.

Taking the centerline of magnetic barrier as the boundary, the motor selects one-half of the adjacent poles for ERNM. The overall shape of the motor can be regarded as an equivalent reluctance network model with the same four parts. The part shown in Fig. 2 is the modeling area.

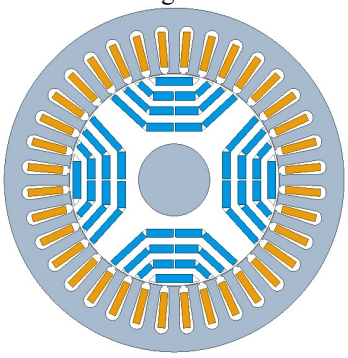

Fig. 1. Model of four-pole PMASynRM.

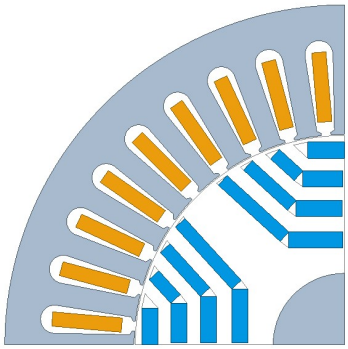

Fig. 2. Modeling area.

In this section, the analytical method of modeling in the modeling area is explained. Besides, the saturation effect of the iron core and the influences of the placement angle of permanent magnet and iron core is also considered.

A. Reluctance Model between Permanent Magnets

According to the structure of PMASynRM as shown in Fig. 1, ERNM has been established. In the previous MEC, the iron core between the magnetic barriers is regarded as a whole reluctance. MEC is to transform the unevenly distributed magnetic field in the motor into an equivalent multi-segment magnetic circuit. In the iron core of the motor, there is a magnetic circuit between the parts where the magnetic potential is different. The magnetic potential of the iron core at different positions between the permanent magnets is different. Therefore, the reluctance between the iron core with magnetic potential difference should be considered when establishing the ERNM, which can reflect the real magnetic field inside the motor and improve the accuracy of the model. In this paper, the iron core was divided into multiple parts: the reluctances in the direction of magnetization between the permanent magnets, and the reluctance in the direction to the air gap.

The model of reluctance established in the iron core is shown in Fig. 3. The model in Fig. 3 considers the reluctance contained in the iron core between two permanent magnets. In Fig. 3, *PM*11 and *PM*21 represent permanent magnets placed horizontally in the middle, and *PM*12 and *PM*22 represent permanent magnets placed at an angle on both sides of the magnetic poles. *R*1, *R*2, *R*3, *R*4, and *R*5 represent the reluctance of the iron core between permanent magnets. Moreover, there is the following relationship between reluctance, *R*1=*R*2, *R*3=*R*4. The reluctances of iron core along the direction of permanent magnet are also built in the model. The reluctance between the permanent magnets *PM*11 and *PM*21 is *R*1, *R*2. Similarly, *R*3 and *R*4 are the reluctance between the permanent magnets *PM*12 and *PM*22. *R*5is the reluctance along the direction from iron core to the air gap. Equation (1) to calculate the value of reluctance.

$$R_n=\frac{L_n}{\mu_s S_n} \tag{1}$$

where L_n and S_n are the length and cross-sectional area of the flux path through the iron core, μ_s is the relative permeability of the iron core.

Since the shape of the iron core of the rotor is not a regular shape, the value of reluctance can be calculated by integral in actual calculations. In the same way, other parts of the motor can also use the above method to solve the reluctance.

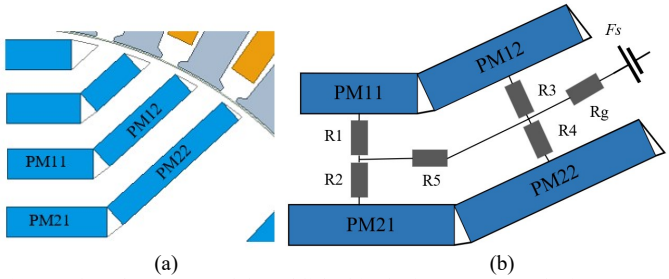

Fig. 3. The reluctance model established in the iron core. (a) The iron core of the rotor and the permanent magnets in the magnetic barrier. (b) The model of the iron core in ERNM.

B. Permanent Magnet Model

During the operation of motor, the MMF and magnetic flux generated by the permanent magnet to the external magnetic circuit are changed, which is difficult to calculate. The permanent magnet can be equivalent to a magnetic flux source in which a constant magnetic flux source is connected in parallel with a constant internal magnetic flux.

Just as the voltage source and current source in the circuit can be equivalently interchanged, the magnetic flux source in the magnetic circuit can also be equivalently transformed into an MMF source.

The total magnetic circuit provided by permanent magnet to the external magnetic circuit can be divided into two parts, one part is linked to the armature winding turns, called the main magnetic flux; the other part is not linked to the armature winding turns, called the leakage flux. In this paper, the leakage flux is considered to be generated in the magnetic flux path between the rotor ribs and the isolation bridge.

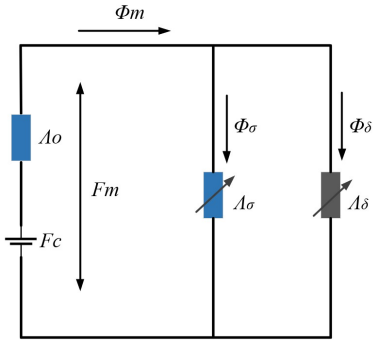

Fig. 4. The equivalent circuit of permanent magnet.

In Fig. 4, Λ_0 represents the internal permeance, and F_c represents the source of MMF, Λ_δ is the main permeance, and Λ_σ is the leakage permeance.

The MMF and reluctance of permanent magnets can be solved according to the following equations:

$$F_c = H_c h_{MP} \tag{2}$$

$$\Lambda_0 = \frac{\mu_r \mu_0 A_m}{h_{MP}} \times 10^{-2} \tag{3}$$

where h_{MP} is the length of the magnetization direction of the permanent magnet, and H_c is the magnetic induction coercive force.

It is considered that permanent magnets also provide MMF for the leakage magnetic circuit. In the leakage magnetic circuit, the flux density of the isolation bridge part is very saturated and the reluctance is large.

$$H_\sigma = \frac{F_c}{l_\sigma} \tag{4}$$

where l_σ is the width of the isolation bridge, and H_σ is the magnetic field intensity of the isolation bridge.

By fitting the magnetization curve of the iron core, the relative magnetic permeability is calculated, and then the leakage reluctance is calculated by (1).

C. ERNM's Other Parameter Calculations

In ERNM, there are MMF generated by armature winding, air-gap reluctance, and stator reluctance, etc. The calculation method of the parameters of these structures in ERNM is introduced below.

1) *MMF of Armature Winding*

The MMF generated by the three-phase motor armature winding can be written as

$$F_s(t,\theta_s) = \sum_{v=6k\pm1} \frac{3}{2} F_{\phi v} \cos(\omega t \mp v\theta_s \mp \theta_0) \tag{5}$$

According to the conversion relationship between stator coordinate system and rotor coordinate system

$$\theta_r = \theta_s - \omega_r t \tag{6}$$

$$\omega_r = \frac{\omega}{p} \tag{7}$$

$$F_s(t,\theta_r) = \sum_{v=6k\pm1} \frac{3}{2} F_{\phi v} \cos(vp\theta_r + (v \mp 1)\omega t \mp \theta_0) \tag{8}$$

where v is the harmonic order, $F_{\phi v}$ is the peak value of MMF harmonic of v order, expressed as:

$$F_{\phi v} = \frac{2\sqrt{2} N k_{\omega v}}{v\pi p} I_s \tag{9}$$

In ERNM, the MMF generated by the armature winding is equivalent to some MMF sources, which can be solved by the integral equation [20].

$$F_{nm}(t,\theta_r) = \frac{1}{\theta_2 - \theta_1} \int_{\theta_1}^{\theta_2} F_s(t,\theta_r) d\theta_r \tag{10}$$

where θ_1 and θ_2 are the angles of the rotor coordinate system, and $F_{nm}(t, \theta_r)$ is the equivalent value of the armature winding's MMF between θ_1 and θ_2 angles.

2) *Air Gap Reluctance*

The MMF drop of air gap is greater in the magnetic circuit of the motor. In ERNM, the air gap of a motor is equivalent to a series of reluctance. Similar to the MMF generated by the armature winding, the air gap is divided into small pieces corresponding to different angles. The small air gap and the corresponding equivalent MMF source are in the same magnetic circuit. The air-gap reluctance calculation does not consider the influence of stator teeth and stator slots. As same as the calculation of iron core reluctance, the air-gap reluctance can be calculated as [20]:

$$R_g = \frac{h_g}{\mu_0 \theta RL} = \frac{h_g}{\mu_0 \times (\theta_2 - \theta_1) \times RL} \tag{11}$$

where h_g is the air-gap width; R is the average radius of the air gap, which is the average value of the stator inner diameter and the rotor outer diameter; L is the lamination stack length; θ is the radian corresponding to the air-gap reluctance on the rotor coordinate system.

3) *Stator Reluctance*

In the magnetic circuit of ERNM, the air gap corresponds to the stator with the same angle. The armature winding contained in the stator is ignored when the stator reluctances were calculated. The radial length of the inner surface and outer surface of the stator is much larger than the air gap. The segmented stator is not a regular rectangle. The integral is used to calculate the stator reluctance. The specific calculation can refer to the calculation of iron core reluctance.

D. Equivalent Reluctance Network Model

In ERNM, the following assumptions are made for the convenience of calculation:

1) End effects are neglected.
2) The outer surface and inner surface of the stator is a magnetic equipotential surface.
3) All materials are isotropic.

ERNM can be derived from the structure of the motor. The values of reluctance and MMF in ERNM are calculated based on the structure of the motor.

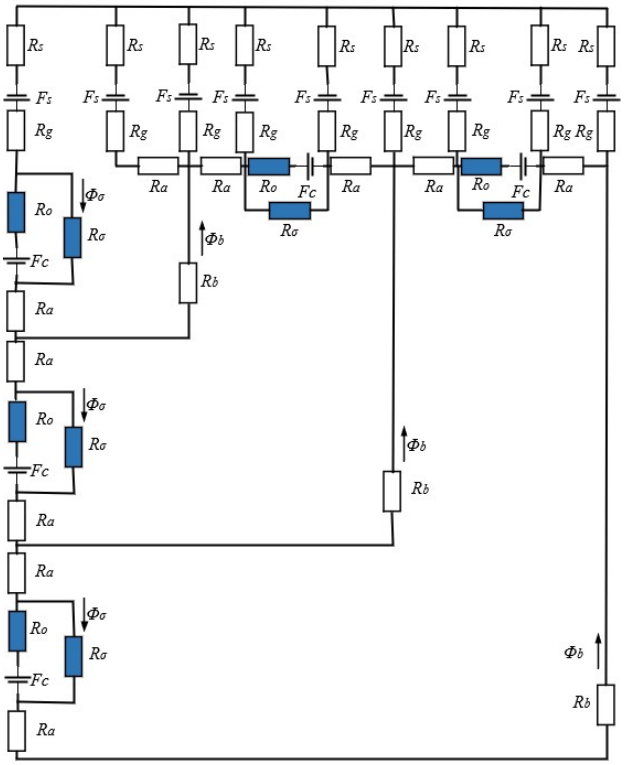

Fig. 5. Schematic diagram of equivalent reluctance network model.

Half of the ERNM diagram is shown in Fig. 5, and the other half can be obtained by symmetry. As shown in Fig. 5, reluctance (R_o, R_σ, R_g, R_s, R_r) denote the reluctance of the permanent magnet, leakage, air gap, stator, rotor, respectively. R_a is the reluctances in the direction of magnetization; $R_{b\,is}$ the reluctance in the direction leading to the air gap.

E. Calculation of Relative Permeability

Due to the effect of the permanent magnet magnetic field, the magnetic field intensity at different positions inside the motor structure will not be same in the operation of the motor. The magnetic induction intensity will change with the change of the magnetic field intensity according to the magnetization curve of iron core. At the same time, the relative permeability of the iron core is constantly changing. This is a difficulty in the calculation, which affects the accuracy of the results of the modeling calculation.

The stator rotates in the rotor coordinate system. The stator reluctance of the same magnetic circuit is smaller than that of the air-gap reluctance. It is assumed that the relative permeability of all stator parts is the same value, and the value of the reluctance of each stator parts is only related to the angle corresponding to the airgap in magnetic circuit. In this way, it is possible to have an accurate model that does not change with the operation of the motor.

The magnetic circuit between different nodes in ERNM is simplified into a branch, and the node electromotive force is simply obtained by the node method, which can be calculated by (12). The saturation of the iron core needs to be considered. The relative permeability of iron core can be calculated as shown in Fig. 6. First, a hypothetical value is set. Secondly, substitute the initial value into ERNM, and get the new relative permeability according to the magnetic flux density. The error between the two values is compared, and the iterative correction calculation is performed until the error is less than a certain value at last.

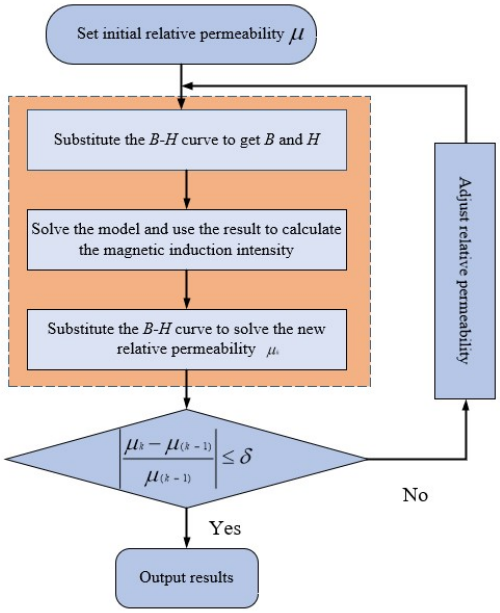

Fig. 6. The calculation flowchart of relative permeability.

$$\begin{pmatrix} R_{11} & R_{12} & \cdots & R_{1n} \\ R_{21} & R_{22} & \cdots & R_{2n} \\ \vdots & \vdots & \ddots & \vdots \\ R_{n1} & R_{n2} & \cdots & R_{nn} \end{pmatrix} \begin{pmatrix} F_1 \\ F_2 \\ \vdots \\ F_n \end{pmatrix} = \begin{pmatrix} \phi_1 \\ \phi_2 \\ \vdots \\ \phi_n \end{pmatrix} \tag{12}$$

In order to simplify the calculation, the motor is divided into the stator part, the part between magnetic barrier, and the part between the magnetic poles. The relative permeability of these three parts is solved by the above method. Dividing the motor into more calculation parts can improve the accuracy of the calculation.

F. The radial and tangential decomposition of the air gap magnetic field

There are two description in the motor: (1) the angle between the permanent magnets in the rotor; (2) the angle between the iron core and the radial direction of the motor.

As shown in Fig. 7, α_1, α_1, and α_3 is the angle between the iron core and the radial direction of the motor. The angle between the permanent magnets also can be seen in Fig. 7.

The air-gap flux density is to solve the magnetic flux density along the radial direction in the motor air gap. The magnetic field in the air gap needs to be expressed as a scalar. After

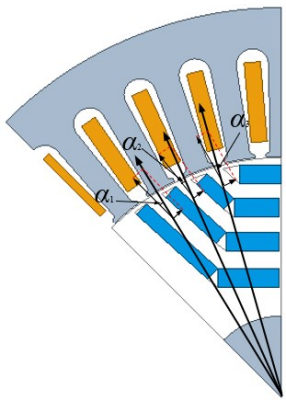

Fig. 7. The angle between the magnetic part between the permanent magnets and the radial direction of the motor.

solving the nodal MMF equations of ERNM, the radial and tangential decomposition of the air-gap magnetic field is based on the motor structure.

III. Calculation of Motor Performance

ERNM can calculate the electromagnetic performance of the motor. According to the solved results, not only the motor performance can be obtained, but also the guidance for the optimal design of the motor performance can be provided.

A. The Air-gap Flux Density

In the above, the method of solving the air-gap magnetic field without considering the influence of stator teeth and stator slots is given. In this paper, a rotor with a smooth surface is used. When calculating the no-load air-gap flux density, the influence of the stator is considered.

The inner surface of the stator is regarded as a magnetic equipotential surface [21],[22]. When the influence of adjacent slots is neglected, the distribution of the air-gap flux density within one slot pitch is shown in Fig. 8.

Taking the centerline of the stator slot as the origin of the coordinate and the air-gap flux density coefficient at the stator teeth as the reference value, the air-gap flux density coefficient within a slot pitch can be expressed as

$$k_{\mathrm{g}}(\alpha_{\mathrm{s}},R)=\begin{cases}1-\beta_{1(\mathrm{r})}-\beta_{1(\mathrm{r})}\cos\dfrac{\pi}{0.8\alpha_{01}}\alpha_{\mathrm{s}}, |\alpha_{\mathrm{s}}|\le 0.8\alpha_{01}\\ 1, 0.8\alpha_{01}\le|\alpha_{\mathrm{s}}|\le\dfrac{\alpha_{\mathrm{t1}}}{2}\end{cases} \tag{13}$$

where α_{s} is the angular position, α_{01} is the slot-width angle,

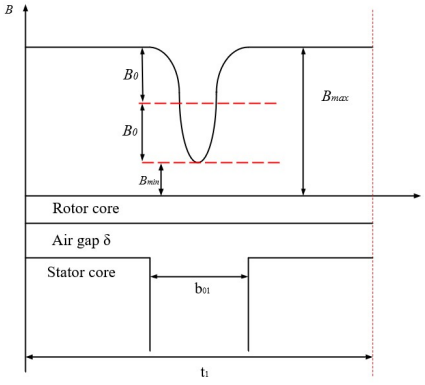

Fig. 8. The distribution of the air-gap magnetic flux density within one slot pitch.

α_{t1} is the slot-pitch angle. α_{01} and α_{t1} can be expressed as

$$\alpha_{01}=\frac{b_{01}}{R_{\text{s-inner}}} \tag{14}$$

$$\alpha_{\mathrm{t1}}=\frac{t_1}{R_{\text{s-inner}}} \tag{15}$$

where R_{s1} is the inner radius of the stator.

$$\beta_{1(\mathrm{r})}=\frac{B_0}{B_{\max}}=\frac{1}{2}\left[1-\frac{1}{\sqrt{1+(\frac{b_{01}}{2\delta})^2(1+\nu^2)}}\right] \tag{16}$$

where ν is the solution of the implicit function.

$\beta_{1(\mathrm{r})}$ in (13) can be calculated by the above formula.

$$y\frac{\pi}{b_{01}}=\ln\left[\frac{\nu+\sqrt{\nu^2+u_1^2}}{u_1}\right]+\frac{2\delta}{b_{01}}\arctan(\frac{2\delta}{b_{01}}\frac{\nu}{\sqrt{\nu^2+u_1^2}}) \tag{17}$$

y and u_1 in (17) can be calculated by the following equation.

$$y=r-R_{\text{s-inner}}+\delta \tag{18}$$

$$u_1=\sqrt{1+(\frac{2\delta}{b_{01}})^2} \tag{19}$$

Simultaneous (13)-(19) can calculate the air-gap flux density coefficient related to the angle position.

After calculating the magnetic flux density of each section of the air gap, multiply the calculation result and the air-gap flux density coefficient to get the no-load air-gap flux density affected by the stator slot.

The no-load air-gap flux density of each section can be expressed as

$$B_{\mathrm{g0}}(\theta_{\mathrm{r}})=k_g(\alpha_s,R)\times\frac{F_{\mathrm{r0}}(\theta_r)\mu_0}{\delta} \tag{20}$$

where $F_{\mathrm{r}}(\theta_{\mathrm{r}})$ is the MMF generated by permanent magnets.

When the motor is under load, the air-gap magnetic field is complicated. The air-gap magnetic field is generated by permanent magnets and armature windings. The armature winding affects the magnetic field inside the motor, which causes the reluctance in the ERNM under load to be recalculated.

In the motor, part of the armature MMF drop is in the air gap, and the other part of MMF drops in other structures of the motor. The matrix can be used to solve the MMF drop between nodes, which can solve the MMF drops in other structures of the motor.

$$B_{\mathrm{gs}}(\theta_{\mathrm{r}})=k_g(\alpha_s,R)\times\frac{\left[F_{\mathrm{s}}(\theta_{\mathrm{r}})-F_{i,j}(\theta_{\mathrm{r}})\right]\mu_0}{\delta} \tag{21}$$

where $F_{\mathrm{s}}(\theta_{\mathrm{r}})$ is the MMF generated by the armature windings, $F_{\mathrm{i,j}}(\theta_{\mathrm{r}})$ is the MMF drop in other structures of the motor.

The air-gap flux density generated by the armature winding can be calculated by (21).

The air-gap flux density under load is generated by permanent magnets and armature windings. The air-gap flux density under load can be expressed as

$$B_{\mathrm{g}}(\theta_{\mathrm{r}})=B_{\mathrm{gs}}(\theta_{\mathrm{r}})+B_{\mathrm{gr}}(\theta_{\mathrm{r}}) \tag{22}$$

where $B_{\mathrm{gs}}(\theta_{\mathrm{r}})$ is the air-gap flux density generated by the

armature windings, $B_{gr}(\theta_r)$ is the air-gap flux density generated by permanent magnets.

B. No-load Back EMF

The no-load back EMF is induced in the armature windings by the no-load air-gap flux generated by the permanent magnets in the motor.

The no-load back EMF of phase A, B, and C can be expressed as

$$E_{A,B,C} = \sum_{i=A,B,C} \frac{NL\omega_r R}{a} B_{g0}(\theta_r) \tag{23}$$

where i is the ith winding of phase A, B, and C, N is the number of turns per coil, a is the parallel-circuits per phase, B_{g0} is the no-load air-gap flux density.

In (23), $B_{g0}(\theta_r)$ is the air-gap flux density at the position of the ith winding in air-gap. Add up the induced EMF of all windings in this phase to get the no-load back EMF of this phase [23].

The flux linkage of the armature windings can be used to solve the no-load back EMF. Equation (24) can also calculate the no-load back EMF.

$$E_{A,B,C} = -\frac{d\phi_{ph=A,B,C}}{dt} \tag{24}$$

In (25), ϕ is the flux linkage of the armature windings. The flux linkage of phase A, B, and C can be expressed as

$$\phi = NLR\int_{\alpha 1}^{\alpha 2} B_{g0}(\theta_r) d\theta_r \tag{25}$$

Both of the above methods can calculate the no-load back EMF. A suitable method can reduce the amount of calculation when using ERNM to analyze the motor.

C. Motor Torque

Motor torque is an important indicator to measure motor performance. Using ERNM to solve the air-gap flux density, the motor torque can be calculated based on the electrical loading. The torque of the motor is a function related to the radian of the rotor and time, which can be obtained by integrating the electric load and the air-gap flux density.

For a given winding, the electrical loading can be expressed as the Fourier series expansion [2].

$$a(\theta_r) = \sum_{v=6k\pm 1} \frac{3\sqrt{2}Nk_{\omega v}}{vp\pi R} I \sin(vp\theta_r + (v \mp 1)\omega t \mp \theta_0) \tag{26}$$

The motor torque T_{em} is calculated by the following integral formula.

$$\begin{aligned} T_{em} &= p\int_0^{2\tau} B_g(\theta_r) a(\theta_r) LR dx \\ &= pR\int_0^{\frac{2\pi}{p}} B_g(\theta_r) a(\theta_r) LR d\theta_r \end{aligned} \tag{27}$$

In the third part, the formula for calculating the motor torque is given. $B_g(\theta_r)$ is the air-gap flux density of the motor under load in (22).

Simultaneous (22), (26), and (27) can calculate the expression of motor torque.

D. Armature Winding Voltage Under Load And Power Factor

The winding voltage under load is an important indicator of the motor, which can be analyzed with the input current to get the power factor.

When the current source is used as the input power source, it is the magnetic flux interlinked with the armature winding under the load. The armature winding voltage can be calculated by its flux linkage. The induced voltage of the armature winding under load is regarded as the armature winding voltage. This approximate calculation method provides a quick solution for the initial design of the motor.

Simultaneous (22), (24), and (25) can get the induced voltage on the armature winding.

There is a certain relationship between the input current and the input voltage of the motor. When the motor input current source is used as the power source, the armature winding voltage contains a large number of harmonics due to the influence of the motor structure and permanent magnets. The difference in the phase angle between the fundamental wave of the armature winding voltage and the current reflects the power factor of the motor. The input current is compared with the armature winding voltage, which can get their phase angle difference and derive the power factor.

IV. Analysis And Comparison

In order to verify the accuracy of the ERNM, a 4p/36s PMASynRM has been analyzed by ERNM and FEM. A two-dimensional FEM model is established based on the structure of the motor. The main structure parameters of machine are shown in Table I. And the FEM model of machine is given in Fig. 1.

In this paper, the relative magnetic permeability of the stator part, the part between magnetic barrier, and the part between the magnetic poles are respectively 0.00775, 0.0087, and 0.00813 under rated load condition.

TABLE I
MAIN STRUCTURE PARAMETERS OF MOTOR

Symbol	Quantity	Value (unit)
P	Rated power	5.5 (kW)
p	Pole number	4
Q	Slot number	36
a	Number of parallel branches	2
N	Number of turns per coil	47
n_N	Rated speed	3000 (rpm)
$R_{s\text{-}inner}$	Inner radius of the stator	65 (mm)
$R_{r\text{-}outer}$	Outer radius of the rotor	64.65 (mm)
R	Radius at the center of the air gap	64.825 (mm)
L	Lamination stack length	60 (mm)
μ_0	Permeability	$4\pi \times 10^{-7}$ H/m

A. The Air-gap Flux Density

In the no-load state of the motor, FEM is used to analyze the air-gap flux density of the motor. The air-gap flux density calculated by FEM and ERNM is compared, as shown in Fig. 9.

In Fig. 9, it can be seen that the results of ERNM are

consistent with those of FEM. The time (3.2s) spent on the calculation by ERNM is less than the time by FEM (3 min 43s). The difference between the analysis results of the no-load air-gap flux density near the middle of the magnetic pole is less than 3%. On both sides of the magnetic pole, the selected air gap segment is larger in ERNM, which increased calculation errors. In the rotor, the magnetic conductive parts between the permanent magnets are respectively the first layer, the second layer, and the third layer from the outside to the inside. The analytical result of the no-load air-gap flux density distribution curve from the third layer of magnetic conductive parts to the edge of the magnetic pole is selected. The integral calculation of the results of FEM and ERNM in this part can get the magnetic flux.

After the integral calculation, it is concluded that the magnetic flux error analyzed by the two methods is less than 5%. The error can be reduced by increasing the section component.

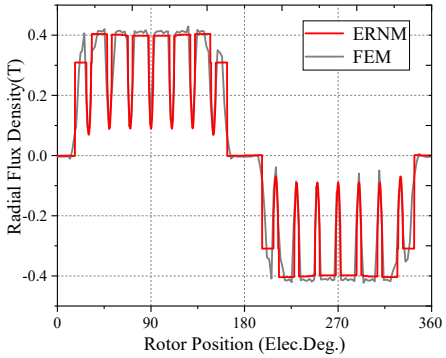

Fig. 9. The distribution of the no-load air-gap flux density within one pair pole.

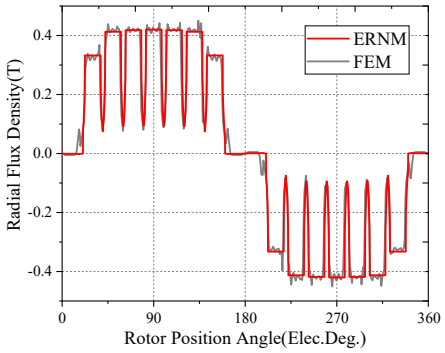

Fig. 10. The distribution of the no-load air-gap flux density within one pair pole when the magnetization length changed.

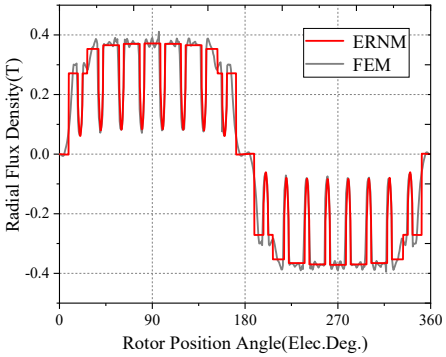

Fig. 11. The distribution of the no-load air-gap flux density within one pair pole when the pole opening angle is 85°.

ERNM also has good performance when the structural parameters of the motor change. In Fig. 10, the length of the magnetizing direction of the permanent magnets in the rotor is changed proportionally. In addition to considering the size of the permanent magnet, the accuracy of ERNM should also be verified at different pole opening angles. Extending the magnetic pole opening angle to a larger angle can verify the accuracy of ERNM within this angle range. When the magnetic pole opening angle of the motor is increased to about 85°, the results of air-gap flux density obtained by ERNM and FEM are shown in Fig. 11. Similarly, the results calculated by the two methods can be integrated to calculate the magnetic flux. Similarly, the results of the two methods can be integrated to calculate the magnetic flux and the respective errors of the two different structural parameters are less than 2%.

Similarly, the values of reluctance in ERNM is recalculated at rated load. The air-gap flux density generated by the permanent magnet and the armature winding are calculated separately. The air-gap flux density under rated load can be calculated by the method introduced in Section III. The distribution of the air-gap flux density under rated load within one pair pole is shown in Fig. 12.

In Fig. 12, ERNM has a good performance when the motor is under load. In ERNM, an equipotential surface of MMF is used as the MMF at a certain rotor position angle. When the motor is under load, the relative permeability of the iron core at different positions is different. ERNM divides the motor structure into three parts to solve the relative permeability, which will cause the error in Fig. 12. The results of ERNM are generally consistent with those of FEM, which has a positive effect on the initial design of the motor.

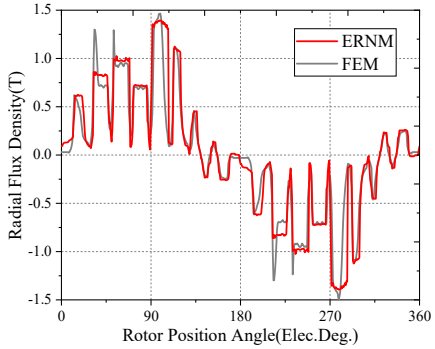

Fig. 12. The distribution of the air-gap flux density under rated load within one pair pole

B. No-load Back EMF

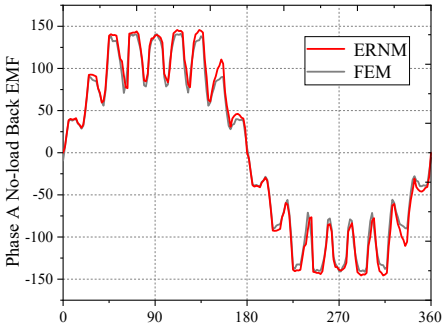

Fig. 13. The no-load back EMF of phase A.

The relationship between the no-load back EMF and the rotation angle of the rotor is shown in Fig. 13.

In Fig. 13, the analytical results of no-load back EMF are calculated at its revolution speed 3000 r/min. The no-load air-gap flux density can be used to solve the no-load back EMF calculation. Moreover, the calculated results are helpful to the analysis of the motor.

C. Motor Torque

When calculating the air-gap flux density under load conditions, it is necessary to consider the influence of the stator slots on the air-gap magnetic field.

Import the data into the equation in the third part, and select a period of torque as a sample to average. Fig. 14 shows the relationship between torque and armature windings current angle. If the ERNM under load does not consider the influence of the armature MMF on the iron core saturation, it will lead to larger errors in the results of ERNM and FEM.

The fundamental MMF generated by the armature current rotates in the air gap at synchronous speed. Calculate the armature MMF at 0s and recalculate the reluctance in ERNM to obtain a more accurate torque. In Fig. 14, the trend of the motor torque with the current angle calculated by ERNM is basically the same as the FEM. Moreover, the results of ERNM calculations can show the influence of the current angle on the torque. The value of the torque will vary with the armature current. When the armature current changes the internal magnetic field of the motor, the armature MMF and the relative permeability of the iron core are different. The reluctance in ERNM needs to be recalculated, which improves the accuracy of the results. Set the current angle of the armature current to 40°, and calculate the torque under different current. The torque

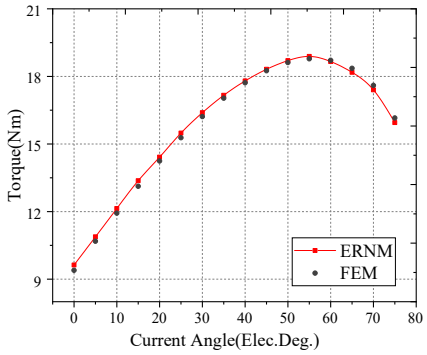

Fig. 14. The distribution of the average torque under different current angles.

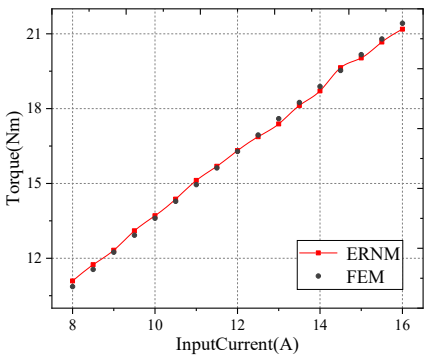

Fig. 15. The distribution of the average torque under different current when current angles at 40°.

under different currents calculated by the proposed ERNM and FEM is shown in Fig. 15.

The section component in ERNM is larger than FEM. Moreover, the relative permeability used when calculating the reluctance in ERNM is obtained by simplified calculation. These are the reasons for the error of the air-gap flux density, and further lead to the error of the torque calculation. However, the error between the calculation results of ERNM and FEM is small. ERNM can reflect the change trend of torque It can be concluded that ERNM reduces the amount of calculation compared with FEM.

D. Armature Winding Voltage Under Load And Power Factor

The induced voltage on phase A is solved by ERNM and FEM. In ERNM, the induced voltage is obtained by using the air-gap flux density under load. The induced voltages solved by FEM and ERNM are shown in Fig. 16.

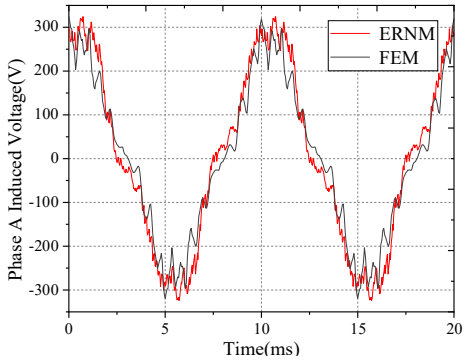

Fig. 16. The induced voltage of phase A is calculated by ERNM and FEM.

The error of the air-gap flux density under load calculated by the two methods is the main cause of the error of the induced voltage. It can be seen from Fig. 16 that the error of the phase A induced voltage calculated by ERNM and FEM is controllable and the calculated induced voltage can still have a very important and constructive significance for the initial design stage of the motor.

The induced voltage and current of Phase A are shown in Fig. 17.

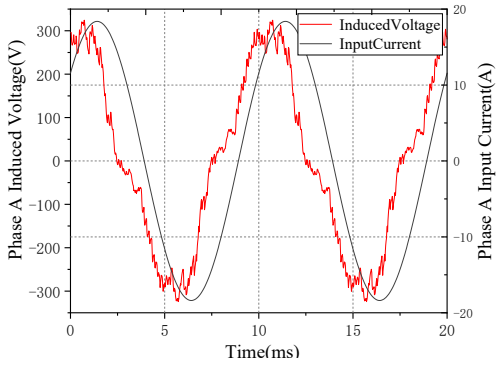

Fig. 17. The induced voltage and input current of phase A.

The induced voltage can be solved by Fourier decomposition to find the phase of its fundamental wave and compare it with the phase of the input current, which can get the power factor of the motor.

TableIIshows the armature winding voltage and power factor

under rated load calculated by ERNM and FEM. The error of the armature winding voltage calculated by ERNM compared with FEM is less than 4%. Although the power factor has errors, it can reflect the performance of the motor in the initial design.

TABLE II
COMPARISON OF ERNM AND FEM

Method	Armature winding voltage	Power factor
ERNM	185.23	0.8173
FEM	178.78	0.8319

V. CONCLUSIONS

In this paper, ERNM is used to calculate the magnetic circuit of PMASynRM. Reluctances also exists in the magnetic circuit between the permanent magnets inside the rotor of PMASynRM, which conforms to the actual distribution of magnetic field inside the motor and were built in ERNM. A solution to the change of the value of reluctance in the model under load is proposed. Through the calculation formula, the no-load air-gap flux density, no-load back EMF, and motor torque are solved. Analytical calculations have been conducted for the 4p/36s PMASynRM. According to the verification by FEM, the ERNM is feasible and effective.

The ERNM has a good coordination between the calculation accuracy and the calculation time. Obviously, ERNM is a method to reduce the amount of calculation and ensure the accuracy of calculation.

Significantly, the ERNM could be applied to analyze other types of motors. Therefore, the ERNM could be widely used for the initial analysis and design of diverse types of motors. And the proposed method can be transformed into a software in the future.

REFERENCES

[1] Y. W. Wang, G. Bacco, N. Bianchi, "Geometry analysis and optimization of pm-assisted reluctance motors," *IEEE Trans. Ind. Appl.,* vol. 53, no. 5, pp. 4338–4347, Sept.-Oct. 2017.

[2] N. Bianchi, S. Bolognani, D. Bon, "Rotor flux-barrier design for torque ripple reduction in synchronous reluctance and pm-assisted synchronous reluctance motors," *IEEE Trans. Ind. Appl.,* vol. 45, no. 3, pp. 921–928, May. 2009.

[3] W. Su, D. Wang, Y. J. Guo, Z. Z. Su, "The DMCM-based analytical calculation of radial vibration force in a nonsalient pole synchronous generator in no-load conditions," *IEEE Trans. Magn.,* vol. 51, no. 5, May. 2015.

[4] L. Zhu, S. Z. Jiang, Z. Q. Zhu and C. C. Chan, "Analytical modeling of open-circuit air-gap field distributions in multisegment and multilayer interior permanent-magnet machines," *IEEE Trans. Magn.,* vol. 45, no. 8, pp. 3121–3130, Aug. 2009.

[5] X. Jin, O. Wasynczuk, G. M. Shaver, "Computationally efficient and flexible magnetic-field-anlysis-based scaling strategy for permanent-magnet machines," *IEEE Trans. Energy Convers.*, vol. 33, no. 3, pp. 1222–1232, Sep. 2018.

[6] M. S. Mirazimi, A. Kiyounarsi, "Magnetic field analysis of multi-flux-barrier interior permanent-magnet motors through conformal mapping," *IEEE Trans. Magn.,* vol. 53, no. 12, Dec. 2017.

[7] C. L. Xia, Z. Zhang, Q. Geng, "Analytical modeling and analysis of surface mounted permanent magnet machines with skewed slots," *IEEE Trans. ind. Electron,* vol. 66, no. 7, Jul. 2019.

[8] C. G. Ma, Y. S. An, H. C. Zhao, S. L. Guo, X. R. Yin, and H. F. Lu, "3-D analytical model and direct measurement method of ultra-thin open-circuit air-gap field of interior permanent magnet synchronous motor with multi-segmented skew poles and multi-layered flat wire windings for electric vehicle," *IEEE Trans. Energy Convers.*, vol. 35, no. 3, pp. 1316–1326, Sep. 2020

[9] F. Chai, H. Y. Hu, L. N. Geng, "Theoretical analysis of torque performance in permanent magnet-assisted synchronous reluctance motor," in *ICEM.,* Aug, 2014.

[10] J. G. Lee, D. K. Lim, H. K. Jung, "Analysis and design of interior permanent magnet synchronous motor using a sequential-stage magnetic equivalent circuit," *IEEE Trans. Magn.,* vol. 55, no. 10, Oct. 2019.

[11] J. K. Si, S. He, W. P. Cao, X. Z. Xu, G. M. Feng, "Electromagnetic characteristics analysis of surface-mounted and interior hybrid PMSM based on equivalent magnetic circuit method," in *IEEE ICEM.,* Aug, 2014.

[12] F. Parasiliti, M. Villani, "Magnetic analysis of flux barriers synchronous reluctance motors," in *IEEE ICEM.,* Sept, 2008.

[13] D. K. Lim, J. S. Ro, "Analysis and design of a delta-type interior permanent magnet synchronous generator by using an analytic method," *IEEE Access.,* vol. 7, pp. 85139–85145, Jun. 2019.

[14] S. H. Han, T. M. Jahns, W. L. Soong, "A magnetic circuit model for an IPM synchronous machine incorporating moving airgap and cross-coupled saturation effects," in *IEEE IEMDC.,* May, 2007.

[15] C. T. Mi, M. Filippa, W. G. Liu, and R. Q. Ma, "Analytical method for predicting the air-gap flux of interior-type permanent-magnet machines," *IEEE Trans. Magn.*, vol. 40, no. 1, pp. 50–58, Jan. 2004.

[16] N. Matsui, M. Nakamura, and T. Kosaka, "Instantaneous torque analysis of hybrid stepping motor," *IEEE Trans. Ind. Appl.*, vol. 32, no. 5, pp. 1176–1182, 1996.

[17] W. B. Tsai and T. Y. Chang, "Analysis of flux leakage in a brush less permanent-magnet motor with embedded magnets," *IEEE Trans. Magn.*, vol. 35, no. 1, pp. 543–547, Jan. 1999.

[18] C. C. Hwang and Y. H. Cho, "Effects of leakage flux on magnetic fields of interior permanent magnet synchronous motors," *IEEE Trans. Magn.*, vol. 37, no. 4, pp. 3021–3024, Jul. 2001.

[19] E. C. Lovelace, T. M. Jahns, and J. H. Lang, "A saturating lumped parameter model for an interior PM synchronous machine," *IEEE Trans. Ind. Appl.*, vol. 38, no. 3, pp. 645–650, 2002.

[20] A. Tessarolo, M. Degano, N. Bianchi, "On the analytical estimation of airgap field in synchronous machine," in *IEEE ICEM.,* Aug, 2014.

[21] Z. Q. Zhu, D. Howe, "Instantaneous magnetic field distribution in brushless permanent magnet DC motors, Part III: Effect of stator slotting," *IEEE Trans. Magn.,* vol. 29, no. 1, pp. 143–151, Jan. 1993.

[22] X. H. Wang, Q. F. Li, S. H. Wang, Q. F. Li, "Analytical calculation of air-gap magnetic field distribution and instantaneous characteristics of brushless DC motors," *IEEE Trans. Energy Convers.*, vol. 18, no. 3, pp. 424–432, Sep. 2003.

[23] C. G. Ma, J. J. Zhang, J. F. Wang, N. Yang, Q. H. Liu, S. G. Zuo, X. D. Wu, P. W. Wang, J. M. Li, J. G. Fang, "Analytical model of open-circuit air-gap field distribution in interior permanent magnet machines based on magnetic equivalent circuit method and boundary conditions of macroscopic equations," *IEEE Trans. Magn.,* vol. 57, no. 3, Mar. 2021.

Changbin Li was born in China on December 1996. He received the B.E. degree in electrical engineering from Shandong University of Science and Technology, Qingdao, China, in 2020. He is currently working toward the M.E. degree in the School of Electrical Engineering, Shandong University, Jinan, China.

His current research interests include design and analysis of permanent magnet-assisted synchronous reluctance motor, motor drive and control on electric vehicle

Xiuhe Wang (Member, IEEE) was born in China on July 1967. He received the B.E. and M.E. degrees in electrical engineering from Shandong University, Jinan, China, in 1989 and 1993, respectively, and the Ph.D. degree in electrical engineering from Shenyang University of Technology, Shenyang, China, in 1996.

From 2001 to 2002, he was a Postdoctoral Fellow with Seoul National University, Seoul, South Korea. Since 2000, he has been a Professor with the School of Electrical Engineering, Shandong University, Jinan, China. His research interests include permanent magnet machines, theoretical analysis and calculation of electromagnetic devices, and artificial intelligence and its application on electrical machines. He has authored/coauthored more than 100 papers on these topics.

Feng Liu was born in China on November 1997. He received the B.E. degree in electrical engineering from Qingdao University, Qingdao, China, in 2020. He is currently working toward the Ph.D. degree in the School of Electrical Engineering, Shandong University, Jinan, China.

His current research interests include design and analysis of permanent magnet machines, motor drive and control on electric vehicle.

Zezhi Xing was born in China on August 1994. He received the B.E. degree from the Shenyang University of Technology, Shenyang, China, in 2016, and the M.E. degree from Shandong University, Jinan, China, in 2019. He is currently working toward the Ph.D. degree in the School of Electrical Engineering, Shandong University, Jinan, China.

His current research interests include design and analysis of the special electrical machines, electromagnetic vibration and control.

Jie Ren received the B. E. and M. S. degrees in control science and engineering from North China Electric Power University, Beijing, China, in 2014 and 2017, respectively. He is currently working toward the Ph.D. degree in electrical engineering from Shandong University, Jinan, China.

His current research focuses on the analytical analysis of permanent magnet machines.

Xinwei Gu was born in China, in June 1996. He received the B.E. degree from University of Liverpool, Liverpool, UK, in 2018, and the MSc degree, in 2019 from University of Sheffield, Sheffield, UK. Now he is currently studying toward the Ph.D degree with the School of Electrical Engineering in Shandong University.

He interests in design and analysis of the permanent magnet motor.